Supporting Information Uphoff et al. Single-molecule DNA repair in live bacteria

1. Construction and characterization of photoactivatable mCherry (PAmCherry) fusion strains. PAmCherry (1) fusion strains of DNA polymerase I (Pol), DNA ligase (Lig), and Fis protein, expressed from their native promoter in *E.coli* AB1157, were generated by replacing the polA, ligA, and fis genes by their PAmCherry fusion versions as described (2). Genes coding for PAmCherry1 and Kanamycin resistance cassette were amplified from the plasmid pROD85 (carrying an 11aa linker preceding PAmCherry and followed by frt flanked kan), using primers with 40-50 nt overhangs homologous to the insertion site at the chromosome (Supplementary Table 1). DNA fragments were treated with DpnI and ~1 µg was used for electroporation of AB1157 cells overexpressing lambda-Red proteins from pKD46 (3). Correct insertion of the fragment into the chromosome was evaluated by PCR using primers flanking the insertion site (Table S1). The growth rates in LB and M9 glycerol medium as well as methyl methanesulfonate (MMS, Sigma) sensitivity were the same for AB1157 wild-type and fusion strains (Table S2 and Fig. S1).

2. Cell preparation for microscopy. Strains were streaked onto LB plates with 25 µg ml^{-1} kanamycin. Single colonies were inoculated into LB and grown at 37ºC for 4-5 h, then diluted 1:10,000 into M9 medium (M9 salts, MEM amino acids + proline, MEM vitamins, 0.2% glycerol) and grown overnight at 37ºC to OD 0.4-0.6. The following morning, cultures were diluted to OD of 0.025 in M9 medium and grown for 2 h at 37ºC to early exponential phase (OD ~ 0.1). Cells were centrifuged and immobilized on agarose pads between two glass coverslips (1.5 thickness, burned to remove any fluorescent background particles). We prepared 1% agarose pads by mixing low-fluorescence 2% agarose in dH_2O 1:1 with 2x M9 medium. For DNA damage experiments, MMS was diluted into M9 medium before mixing with agarose solution. We used 100 mM MMS in all experiments; the lowest concentration that resulted in saturated Pol and Lig binding. For Fig. 4*E* we used 25 - 200 mM MMS. The adaptive response was induced by 3 mM MMS treatment in liquid M9 culture at 37ºC for 1 h (Fig. S1 shows that this MMS concentration is non-lethal); adapted cells were subsequently prepared for imaging on 100 mM MMS agarose pads identical to the damage response experiments with non-adapted cells in Fig. 5*A*. For DNA damage recovery experiments, cells were immobilized using 1% polyethylenimine on glass coverslips with silicon gaskets. This allowed imaging in M9 medium first, then incubating with M9 medium + 100 mM MMS for 15 min, followed by removal of MMS and washing with M9 medium to allow recovery. For fixation, centrifuged cells prepared as above were resuspended into 2.5% paraformaldehyde in PBS buffer and fixed for 45 min shaking at 22ºC. Fixed cells were washed with PBS and immobilized on agarose pads as above.

3. Microscope setup. PAmCherry fusion proteins were imaged on a custom-built total internal reflection fluorescence (TIRF) microscope with a 561 nm laser (SLIM-561 200 mW, Oxxius) and photoactivated with a 405-nm laser (MLL-III-405 100 mW, CNI). The 561-nm and 405-nm laser beams were coupled into the same single-mode optical fiber. At the fiber output, the laser beams were collimated and focused (100x oil immersion objective, NA 1.4, Olympus) onto the sample under an angle allowing for highly inclined thin illumination (4). Fluorescence emission was filtered by a dichroic mirror and notch filter (ZT405/473/561rpc & ZET405/473/561NF, Chroma). PAmCherry emission was projected onto the central region of an EMCCD camera (iXon 897, 512x512 pixels, Andor) using a custom-built triple view component (T540lpxr & T640lpxr, Chroma). The pixel size was measured as 114.5 nm. Cell outlines were recorded with an LED source (pE-100, coolLED) in an Olympus condenser (IX-2, Olympus). Sample position and focus were controlled with a motorized stage and z-motor (MS-2000 and LS-50, ASI Imaging).

4. Data acquisition. PALM movies were recorded under continuous 400 $W \cdot cm^{-2}$ 561-nm excitation at 15.26 ms/frame for 7,500 or 10,000 frames; transmitted light microscopy images of the cell outlines were acquired before PALM imaging. Photoactivating less than one PAmCherry fluorophore per cell at any time was controlled by adjusting the 405-nm excitation (from 0 - 1 $W \cdot cm^{-2}$) over the duration of the movie. We confirmed cell viability after PALM imaging (Fig. S1). Using cells immobilized on agarose pads with rich defined medium (Teknova), we followed normal cell growth and division on the microscope slide at room temperature for 45 min. We subsequently imaged Pol-PAmCherry with standard acquisition and excitation conditions. After PALM imaging, cells continued normal growth, but we noticed a 15-20 min time lag before growth continued. 67 out of 70 imaged cells (95.7%) recovered growth, showing no further sign of light-induced DNA damage.

5. Data processing. Localization analysis was performed using custom-written MATLAB software (MathWorks), adapted from Refs. 5 and 6. PSFs were identified for localization by band-pass filtering and applying an intensity threshold to each frame of a super-resolution movie. Candidate positions were used as initial guesses in a two-dimensional elliptical Gaussian fit for high-precision localization. Free fit parameters were x-position, y-position, x-width, y-width, elliptical rotation angle, intensity, background. Single-particle tracking analysis was performed by adapting the MATLAB implementation of the algorithm described in Ref. 7. Positions were linked to a track if they appeared in consecutive frames within a window of 5 pixels (0.57 μm) for Pol and Lig; this window size ensures 98% of steps are correctly linked for an apparent diffusion coefficient of 1 $\mu m^2 \cdot s^{-1}$. The tracking window for Fis was 8 pixels (0.92 μm). In rare cases when multiple localizations fell within the tracking radius, tracks were linked such that the sum of step distances was minimized. We used a memory parameter of 1 frame to allow for transient disappearance of the PSF within a track due to blinking or missed localization.

6. Diffusion analysis of single-molecule tracks. We distinguished bound and diffusing proteins by calculating an apparent diffusion coefficient $D^* = MSD/(4\,\Delta t) - \sigma_{loc}^2/\Delta t$ from the mean-squared displacement (MSD) for each track with a minimum of 4 steps, correcting for the localization standard deviation of 40 nm. Shorter tracks were discarded for this analysis because the statistical error prohibits clear separation of bound and diffusing proteins. Histograms of D^* show a peak at $D^* \sim 0\ \mu m^2 \cdot s^{-1}$ for the bound molecules and a separate distribution for the diffusing molecules, the width of which matched simulated data (Fig. S4). We note that D^* is an apparent diffusion coefficient, used to identify bound and diffusing molecules, and does not equal an accurate diffusion coefficient because of cell confinement and motion blurring (8); instead, we simulated Brownian motion and modelled PALM movies to find the input diffusion coefficient that reproduced observed experimental data (see below). Guided by the D^* distributions in fixed cells, we set two thresholds $D^* < 0.15\ \mu m^2 \cdot s^{-1}$ for MSD(Δt=15.26ms) and $D^* < 0.075\ \mu m^2 \cdot s^{-1}$ for MSD(Δt=30.52ms) to identify bound tracks. The percentage of bound molecules was calculated from the number of bound tracks divided by the total number of tracks with 4 or more steps. Binding distributions across cells were measured by identifying the fraction of bound molecules within manually segmented cells.

Using simulated data of a single diffusing species matching experimental data (see below), we estimated false positive identification of bound tracks (erroneous bound identification of diffusing molecules) to 0.7%. Using simulations of a mixed population of bound and diffusing tracks (containing 15% of tracks with $D = 0\ \mu m^2 \cdot s^{-1}$) we also estimated a false negative identification (missed identification of a bound track) of 1.1%.

Complete repair events in our experimental data (Fig. 3*A-C*, Fig. S6) were identified in tracks that showed diffusion flanking a full binding event by calculating a time trace of D^* over all steps of a track. Only tracks with 12 or more steps were included in this analysis. 1.1% of 3700 analyzed Pol traces showed complete binding events in MMS damaged cells; whereas 0.2% of ~2200 Pol traces in undamaged cells, respectively. This reflects the ~5 fold increase of Pol binding with MMS.

7. Simulations. We simulated three-dimensional Brownian motion with diffusion coefficient D by creating random steps in x, y, and z directions. The step length in each direction was drawn from a Gaussian distribution with zero mean and variance $2D \cdot dt$, with a simulation time step $dt = 0.1526$ ms (100 time steps per 15.26-ms frame). The population of immobile tracks was generated by randomly generating individual tracks with $D = 0\ \mu m^2 \cdot s^{-1}$ for the whole duration of the track, such that the average percentage of immobile tracks matched experimental results of 2.7% bound Pol and 3.8% bound Lig in undamaged cells. The rod-shaped three-dimensional confinement was approximated by a cylinder with spherical caps (2 μm length, 0.65 μm diameter); this area accounts for confinement to the nucleoid rather than the whole cytoplasm, as can be seen in Fig. 1*F* and Fig. S2. Initial molecule positions were uniform within the confinement. Steps that would lead outside the confinement were rejected. For stochastic photoactivation and bleaching, single tracks started at random times uniformly distributed over the total number of time steps and each track length was drawn from an exponential distribution with an experimentally determined mean duration of 54 ms. We simulated 400 tracks per cell in 152 s long movies (10^6 time steps) such that the density of activated particles was similar to experiments.

To accurately model the raw experimental fluorescence data including motion blurring, PSFs were centred on each position of the simulated Brownian motion tracks that were projected onto the x-y plane. Matching our experimental frame rate, every 100 simulation time steps were integrated to form a frame of a movie

with 10,000 frames in total. Simulation parameters for the confinement volume, PSF intensity, PSF width, background noise per pixel, number of frames per movie, number of molecules per cell, and mean number of frames per track were chosen to match experimental values. Simulated movies were saved for localization, tracking, and further data analysis (MSD curves, cumulative distribution curves, *D** distributions), performed exactly the same as for experimental data.

To evaluate whether simple Brownian motion with a bound population matches experimental observations and to extract accurate diffusion coefficients, we performed simulations for a range of diffusion coefficients D = 1.5 - 5.5 $\mu m^2 \cdot s^{-1}$ with increments of 0.1 $\mu m^2 s^{-1}$. Simulation results were evaluated by calculating the squared deviation between simulated and experimental data based on MSD curves, cumulative distribution curves, and *D** distributions. The best parameter estimate for the accurate diffusion coefficient D was obtained from the minimum of the squared deviation values (least squares estimate). We found diffusion coefficients D_{Pol} = 2.7 ± 0.4 $\mu m^2 \cdot s^{-1}$ and D_{Lig} = 3.5 ± 0.3 $\mu m^2 \cdot s^{-1}$ from simulations that precisely matched experimental data (Fig. S4). These results are consistent with previous reports for proteins of similar size (9, 10). Because of confined diffusion and motion blurring, *D** distributions peak at lower values D^*_{Pol} ~ 0.8 $\mu m^2 \cdot s^{-1}$ and D^*_{Lig} ~ 1 $\mu m^2 \cdot s^{-1}$, as for experimental data.

The nucleoid-association indicates non-specific DNA-binding of Pol and Lig in vivo. On the other hand, their diffusion in undamaged cells is consistent with ordinary Brownian motion. Taken together, these two findings suggest that Pol and Lig interact transiently with DNA, on a time-scale shorter than our exposure time (15 ms/frame). Multiple cycles of binding and diffusion per frame result in a Gaussian distribution of displacements characteristic of Brownian motion. The combination of three-dimensional diffusion and one-dimensional sliding on DNA can facilitate the search for specific DNA sites (11); however, the relative non-specific binding and diffusion times in vivo remain unknown for most proteins, including Pol and Lig. Our observation of weak non-specific binding is in agreement with the requirement of a primer-template DNA structure for tight binding of Klenow fragment in vitro (12-14). Similarly, the affinity of DNA ligases for dsDNA appears to be much weaker than binding to a nicked DNA substrate (15, 16).

8. Binding-time distributions using long exposure times. PALM movies to measure binding times with reduced photobleaching were recorded at low continuous 561-nm excitation intensities (40 $W \cdot cm^{-2}$, 60 $W \cdot cm^{-2}$, and 80 $W \cdot cm^{-2}$) using long exposure times (500.26 ms/frame, 750.26 ms/frame, and 1000.26 ms/frame). Bound and diffusing molecules were distinguished by the mean PSF width over each track, with thresholds x-width < 160 nm and y-width < 200 nm to identify bound molecules (Fig. *3D-F*, Fig. S7*A-G*). Note that the percentage of bound molecules under these conditions appears larger than for short exposure times since this approach focuses mainly on the bound molecules and their binding-time distribution, which is defined by the duration of tracks that passed the width thresholds. The probability of observing a particular on-time is the product of the underlying binding-time probability and the bleaching probability. The bleaching-time distributions were measured independently using Pol-PAmCherry in fixed cells with the same acquisition and excitation conditions (Table S3). On-time and bleaching-time distributions were fitted with single-exponential functions to extract exponential-time constants t_{on} and t_{bleach}, and the binding-time constant was calculated by $t_{bound} = t_{on} \cdot t_{bleach} / (t_{bleach} - t_{on})$.

Stochastic photoactivation of molecules before or during binding events does not influence our measurement, because the observed binding times follow an exponential distribution and are therefore memoryless. We confirmed that the bleaching rates in fixed cells and live cells were the same by using a PAmCherry fusion protein that unbinds DNA much slower than photobleaching, such that the observed on-time distribution in live cells equals the bleaching-time distribution. The Structural Maintenance of Chromosomes complex in *E.coli*, MukBEF, binds DNA in 1-3 large clusters per cell with a turnover rate of ~50 s (17). Localizations of bound MukE-PAmCherry were at the expected positions and the on-time distribution at 1-s exposure and 40 $W \cdot cm^{-2}$ excitation was essentially identical to the bleaching-time distribution from Pol-PAmCherry in fixed cells under the same exposure and excitation conditions (Fig. S7*H*).

9. Protein copy number measurements. To obtain protein copy numbers per cell (Fig. 4*A*, Fig. S8), we ensured activation of essentially all PAmCherry molecules by acquiring long movies (up to 20,000 frames; lasting for 5 min) with a constant photoactivation rate by increasing 405-nm excitation gradually (18). We used highly inclined thin illumination (4) to image the majority of molecules within ~0.8 μm thick cells. Any

residual excitation gradient will not affect molecule counts in live cells because all diffusing molecules will get activated and imaged when they move into the excitation/activation field. We manually segmented cell outlines in transmitted light microscopy images to determine the number of tracks within each cell. Cells were split if a septum was clearly visible in the transmitted light microscopy image. On the basis of the PAmCherry maturation time of 23 min (1) and a steady-state cell generation time of ~120 min in M9 glycerol at room temperature, we estimated a molecule detection efficiency of ~80%. In fixed cells, Pol counts were 20% lower than in live cells.

10. Estimating repair rates, search times, and substrate numbers. Using the measured binding times, we calculated the search time from the fraction of bound molecules:
$N_{bound}/(N_{bound}+N_{free}) = t_{bound}/(t_{bound}+t_{search})$.
The repair rate per molecule is given by
$r = 1 / (t_{bound} + t_{search})$.
The total repair rate per cell for a given copy number N_{copies} is
$r_{cell} = N_{copies} \cdot r$.
The diffusion-limited search time of a single enzyme with diffusion coefficient, D, for free substrates with concentration, $C_{substrate}$, and association radius, a, is given by Ref 11:
$t_{search} = 1 / (4 \pi \cdot D \cdot a \cdot C_{substrate})$.
Using $C_{substrate} = N_{substrate}/V_{e.coli}$, we calculate the number of free substrates:
$N_{substrate} = V_{e.coli} / (4 \pi \cdot D \cdot a \cdot t_{search})$.
We use parameter values $V_{e.coli} = 10^{-18}$ m^3; $D_{Pol} = 2.7$ μm^2·s^{-1} and $D_{Lig} = 3.5$ μm^2·s^{-1} (see simulations); $a = 0.5$ nm; $t_{search} = 14$ s for Pol and $t_{search} = 9$ s for Lig (with saturating MMS).
This gives $N_{substrate} = 4.2$ for Pol, and $N_{substrate} = 5.1$ for Lig.
We further calculate the lifetime of a free substrate before enzyme binding:
$t_{free} = V_{e.coli} / (4 \pi \cdot D \cdot a \cdot N_{enzymes})$
$N_{enzymes}$ refers to the number of free enzymes that are available for substrate binding, accounting for the fraction of enzymes already bound. We obtained this fraction from our measurements at saturating MMS (Table 1): $N_{enzymes} = 479 - 62 = 417$ for Pol, and $N_{enzymes} = 226 – 40 = 186$ for Lig.
The lifetime of gapped substrates, considering only Pol binding, gives $t_{free} = 140$ ms. With Pol and Lig both competing for nicked substrates, we find $t_{free} = 90$ ms.
Alternatively, we can use the fact that the turnover rate of free substrates equals the enzyme repair rate r_{cell} (Table 1) at equilibrium:
$r_{cell} = N_{substrate} / t_{free}$.
Using $r_{cell} = 29.7$ s^{-1} for Pol, and $r_{cell} = 19.2$ s^{-1} for Lig gives the same results for t_{free}.

11. Estimating MMS damage rates from published data. An in vitro method for quantification of DNA methylation damage has been reported (19). The authors measured 47 7meG lesions per 10^4 bases after 25 mM MMS treatment for 60 min. Considering that 7meG accounts for 83% of all MMS lesions, this gives a total damage rate of 430 lesions·chromosome^{-1}·min^{-1}. Consistent with this, early in vivo work showed that 60 min treatment with 25 mM radioactively labelled MMS causes methylation of 0.6% of DNA bases in *E.coli* (20). This gives an estimate for the damage rate of 460 lesions·chromosome^{-1}·min^{-1}. These numbers can be compared to our measured ligation rate, which is expected to equal the rate at which lesions are generated under non-saturating MMS concentrations in steady state. Using the Lig rate at 25 mM MMS (Fig. 4E) and subtracting the basal reaction rate gives a repair rate of 469 ± 136 reactions·cell^{-1}·min^{-1}.

12. Discussion on potential aggregation and localization artifacts of fluorescent fusion proteins. It has been shown that fluorescent protein fusions can aggregate in cells (21) and may create artifacts in protein localization (22). We closely inspected our data in this respect and found that all characteristics of the tracking data exclude localization artifacts or aggregation of the PAmCherry fusion proteins in live *E.coli*: (i) The majority (>95%) of Pol, Lig, and Fis showed rapid diffusion in undamaged live cells; (ii) The MSD and cumulative distribution curves scaled with the expected individual molecular weights of the Pol, Lig, and Fis fusion proteins; (iii) Protein localizations were distributed over a large area in the cell corresponding to the nucleoid without any sign of clustering; (iv) Simulations showed that the observed diffusion is consistent with ordinary Brownian motion and the extracted diffusion coefficients for Pol and Lig matched those of other proteins with similar molecular weight; (v) We did not observe any change in MMS sensitivity of strains carrying Pol or Lig PAmCherry fusions compared to wild type as would be caused by aggregation or localization artifacts; (vi) Bound tracks of Pol III-PAmCherry (ε subunit) were localized exclusively at the

expected positions of the replication fork in live *E.coli*, while diffusing Pol III were distributed throughout cells; there was no sign of binding, sticking, or aggregation at other positions in the cell; (vii) Tracking MukBEF-PAmCherry fusions in live *E.coli* also showed bound molecules only at positions in the cell that were previously observed using different fluorophores (17).

References

1. Subach FV et al. (2009) Photoactivatable mCherry for high-resolution two-color fluorescence microscopy. *Nat Methods* 6(2):153-159.
2. Reyes-Lamothe R, Possoz C, Danilova O, Sherratt DJ (2008) Independent positioning and action of Escherichia coli replisomes in live cells. *Cell* 133(1):90-102.
3. Datsenko KA, Wanner BL (2000) One-step inactivation of chromosomal genes in Escherichia coli K-12 using PCR products. *Proc Natl Acad Sci USA* 97(12):6640-6645.
4. Tokunaga M, Imamoto N, Sakata-Sogawa K (2008) Highly inclined thin illumination enables clear single-molecule imaging in cells. *Nat Methods* 5(2):159-161.
5. Holden SJ et al. (2010) Defining the limits of single-molecule FRET resolution in TIRF microscopy. *Biophys J* 99(9):3102-3111.
6. Holden SJ, Uphoff S, Kapanidis AN (2011) DAOSTORM: an algorithm for high-density super-resolution microscopy. *Nat Methods* 8(4):279-280.
7. Crocker JC, Grier DG (1996) Methods of digital video microscopy for colloidal studies. *J Colloid Interface Sci* 179(1):298-310.
8. Michalet X, Berglund AJ (2012) Optimal diffusion coefficient estimation in single-particle tracking. *Phys Rev E* 85:061916.
9. Elowitz MB, Surette MG, Wolf PE, Stock JB, Leibler S (1999) Protein mobility in the cytoplasm of Escherichia coli. *J Bacteriol* 181(1):197-203.
10. Nenninger A, Mastroianni G, Mullineaux CW (2010) Size dependence of protein diffusion in the cytoplasm of Escherichia coli. *J Bacteriol* 192(18):4535-4540.
11. Halford SE, Marko JF (2004) How do site-specific DNA-binding proteins find their targets? *Nucl Acids Res* 32(10):3040-3052.
12. Turner RM jr, Grindley, NDF, Joyce CM (2003) Interaction of DNA Polymerase I (Klenow fragment) with the single-stranded tremplate beyond the site of synthesis. *Biochemistry* 42(8):2373-2385.
13. Datta K, Wowor AJ, Richard AJ, LiCata VJ (2006) Temperature dependence and thermodynamics of Klenow polymerase binding to primed-template DNA. *Biophys J* 90(5):1739-1751.
14. Wowor et al. (2010) Thermodynamics of the DNA structural selectivity of the Pol I DNA polymerases from Escherichia coli and Thermus aquaticus. *Biophys J* 98(12):3015-3024.
15. Cherepanov AV, de Vries S (2002) Dynamic mechanism of nick recognition by DNA ligase. *Euro J Biochem* 269(24):5993-5999.
16. Rossi R, Montecucco A, Ciarrocchi G, Biamonti G (1997) Functional characterization of the T4 DNA ligase: a new insight into the mechanism of action. *Nucl Acids Res* 25(11):2106-2113.
17. Badrinarayanan A, Reyes-Lamothe R, Uphoff S, Leake MC, Sherratt DJ (2012) In vivo architecture and action of bacterial Structural Maintenance of Chromosome proteins. *Science* 338(6106):528-531.
18. Lee SH, Shin JY, Lee A, Bustamante C (2012) Counting single photoactivatable fluorescent molecules by photoactivated localization microscopy (PALM). *Proc Natl Acad Sci USA* 109(43):17436-17441.
19. Fundador E, Rusling J (2007) Detection of labelled abasic sites in damaged DNA by capillary electrophoresis with laser-induced fluorescence. *Anal Bioanal Chem* 387(5):1883-1890.
20. Lossius I, Krüger PG, Kleppe K (1980) Effect of methyl methanesulfonate on the nucleoid structure of Escherichia coli. *J Gen Microbiol* 124(1):159-171.
21. Landgraf D, Okumus B, Chien P, Baker TA, Paulsson J (2012) Segregation of molecules at cell division reveals native protein localization. *Nat Methods* 9(5):480-482.
22. Swulius MT, Jensen GJ (2012) The Helical MreB cytoskeleton in Escherichia coli MC1000/pLE7 is an artifact of the N-terminal yellow fluorescent protein tag. *J Bacteriol* 194(23):6382-6386

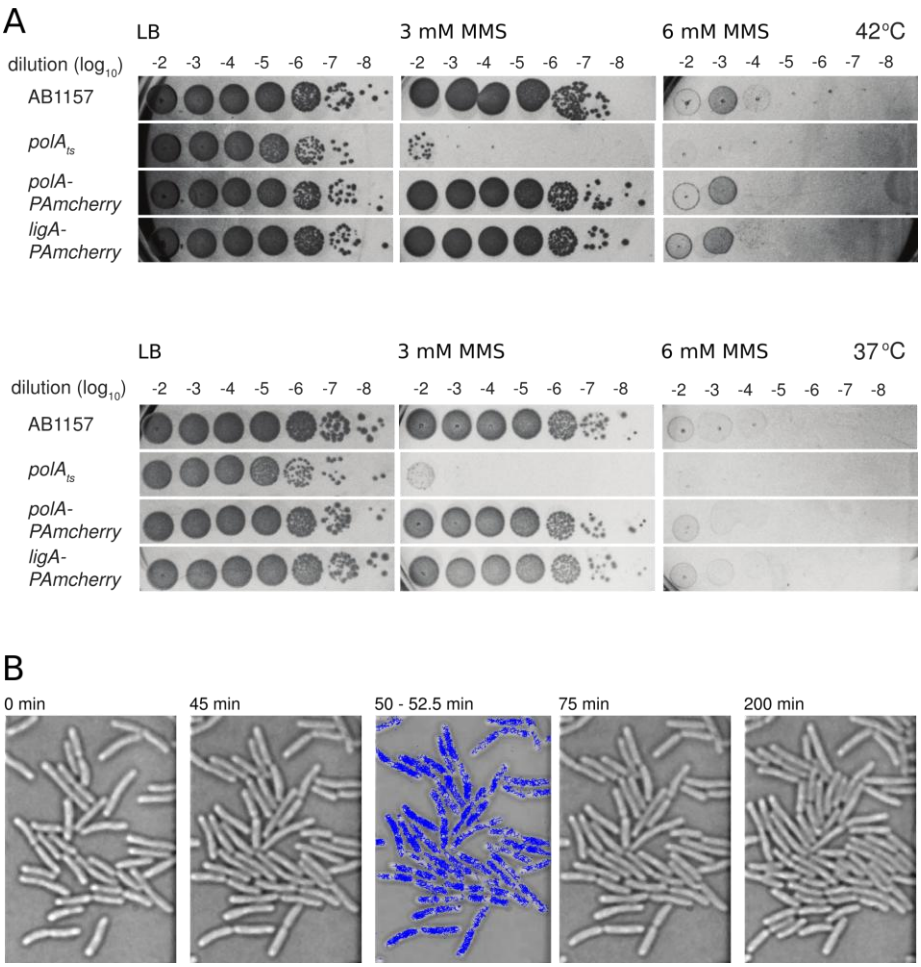

Fig. S1. MMS sensitivity and viability after imaging. (*A*) Serial dilutions of strains were grown overnight on LB agar at 42°C (top), and 37°C (bottom) without MMS (left), 3 mM MMS (middle), 6 mM MMS (right). Wild type AB1157 showed the same MMS sensitivity and growth rates as fusion strains *polA-PAmCherry* and *ligA-PAmCherry*. The temperature sensitive DNA polymerase I mutant strain $polA_{ts}$ was hyper-sensitive to MMS. (*B*) *E.coli* cells are viable after imaging. 0 - 45 min: Cells grow on the slide. 50 - 53 min: PALM imaging of Pol-PAmCherry under standard illumination conditions. 53 - 75 min: Cells halt growth for ~20 min. 75 - 200 min: Cells continue normal growth. 67 out of 70 cells (95.7%) recovered growth, with no sign of light-induced damage.

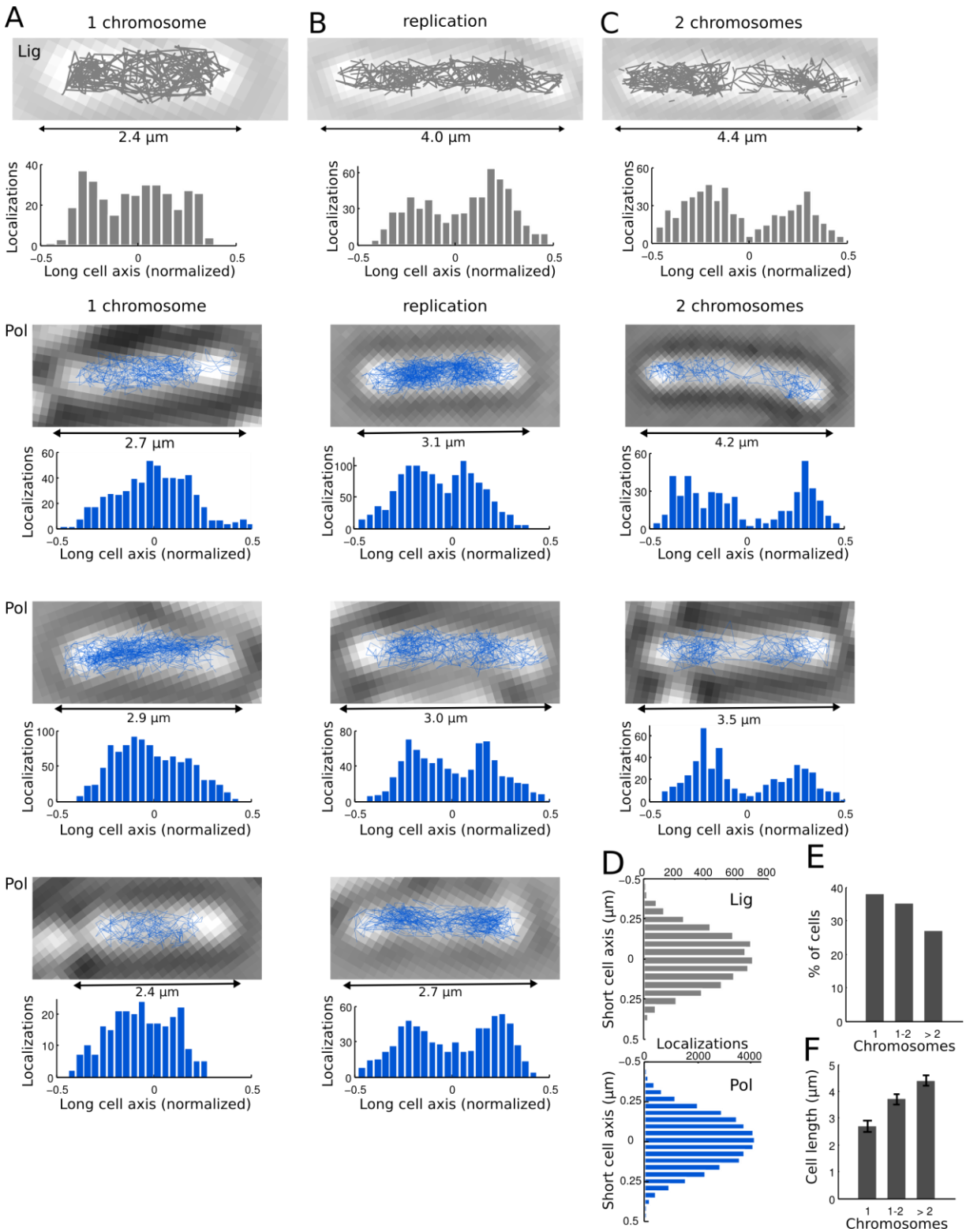

Fig. S2. The spatial distributions of Lig and Pol tracks reflect the organization of the nucleoid in replicating *E.coli*. Tracks are shown in blue/gray, histograms of localizations projected onto the normalized long cell axis are shown underneath together with the cell length. Like the nucleoid, Pol and Lig tracks occupied the central area of the cell, avoiding the cell poles. Chromosome separation is evident from discrete areas of high track density in longer cells. (*A*) Short cells with a single chromosome. (*B*) Medium length cells during replication in the process of chromosome separation. (*C*) Long cells with two separate chromosomes. (*D*) Lig localizations from 20 cells and Pol localizations from 47 cells projected onto the short cell axis, showing the ~0.6 µm width of the nucleoid. (*E*) Based on Pol localization distributions, cells were manually sorted by the number of chromosomes and counted (134 cells). (*F*) Average cell length versus the number of chromosomes (±SEM, 134 cells).

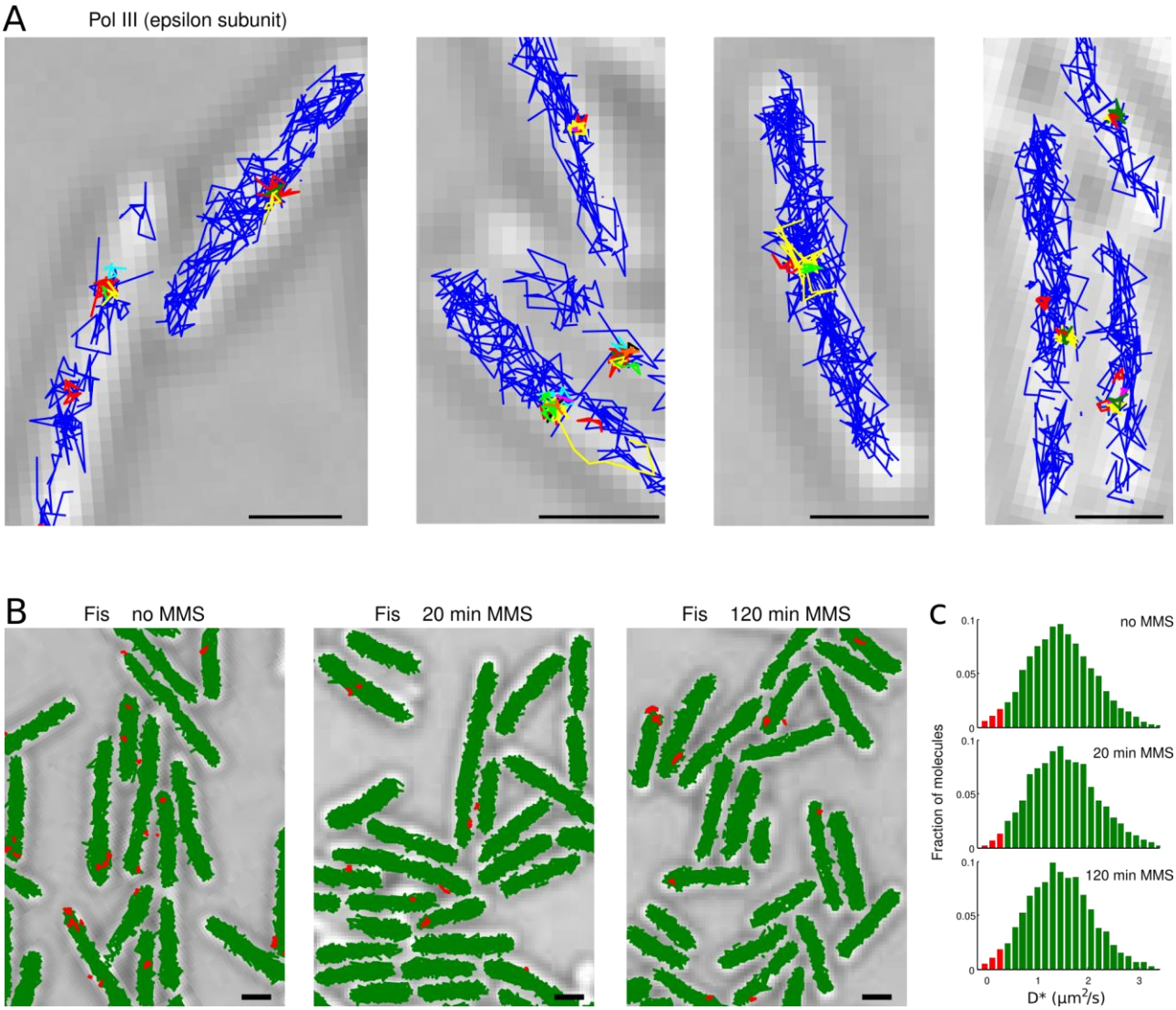

Fig. S3. Single-molecule tracking controls. Scale bars: 1 μm. (*A*) Tracking the ε subunit of Pol III in live *E.coli* as a positive control for DNA-binding. Tracks of molecules that were classified as bound are shown in random colours; all other tracks, corresponding to the diffusing molecules, are shown in blue. The yellow track in the lower quarter of the second panel also displays the search path of a single Pol III molecule. (*B*) Tracking the nucleoid associated protein Fis as control without DNA repair activity. Fis tracks are shown in undamaged cells, 20 min 100 mM MMS-treated cells, and 120 min 100 mM MMS-treated cells. Tracks of diffusing and bound molecules are plotted in green and red, respectively. (*C*) Apparent diffusion coefficient (*D**) distributions corresponding to Fis tracking data in panel *B*. N > 10,000 tracks; populations of bound molecules are shown in red.

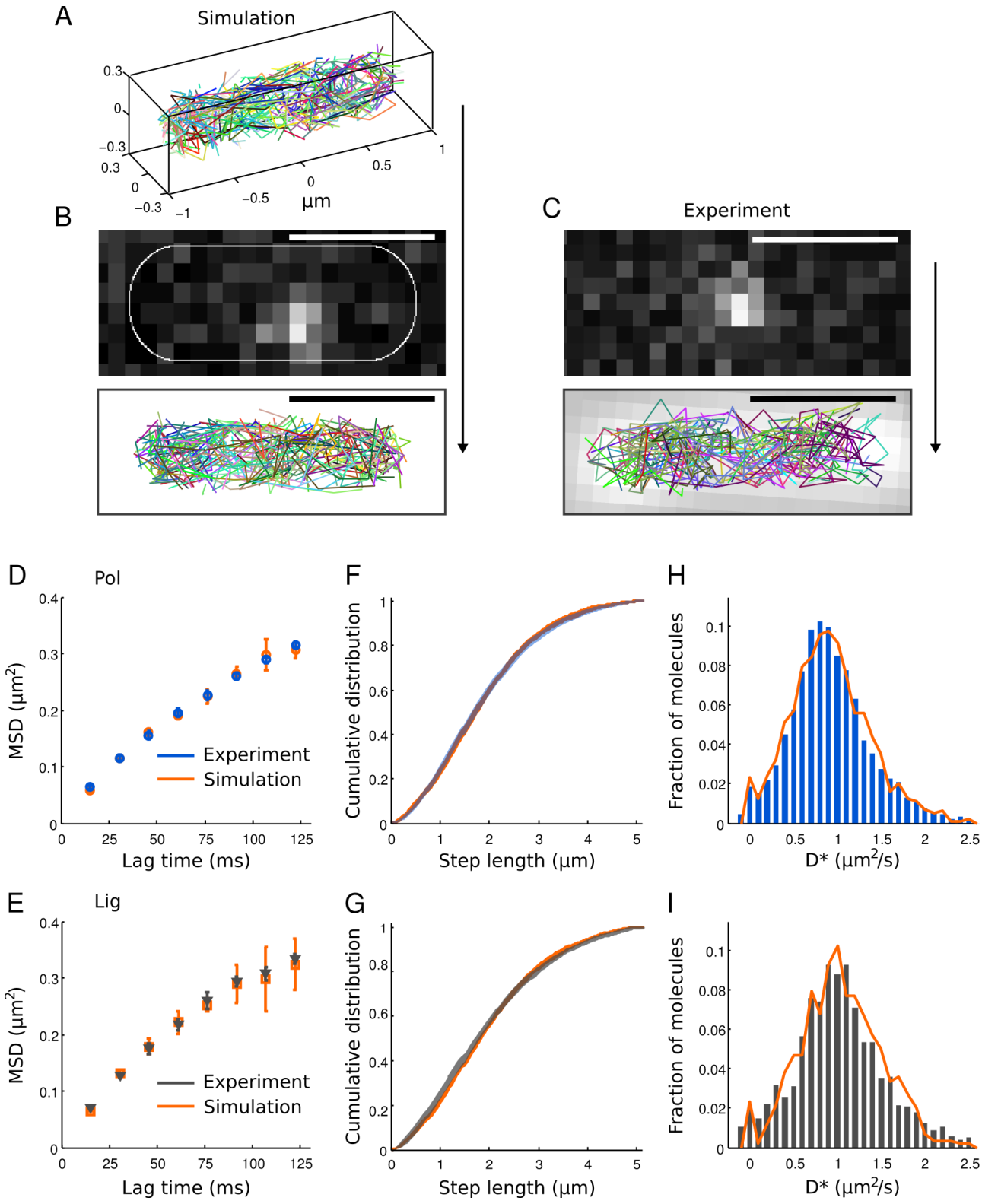

Fig. S4. Pol and Lig diffusion match simulations of Brownian motion with diffusion coefficients D_{Pol} = 2.7 ± 0.4 μm^2·s^{-1} and D_{Lig} = 3.5 ± 0.3 μm^2·s^{-1}. (*A*) Simulated 3D Brownian motion tracks. (*B*) Simulated tracks were used to model PALM movies (example frame shown) for localization and tracking analysis that was performed identical to analysis of experimental data. (*C*) Example frame from an experimental PALM movie and resulting tracks. (*D-I*) Comparison between simulation (orange) and experiment for Pol (blue, *Upper*) and Lig (gray, *Lower*) in undamaged cells: (*D-E*) Mean-squared displacement (MSD) versus lag time (± SD). (*F-G*) Cumulative distributions of the diffusion step length (curve width: ±SD.). (*H-I*) Apparent diffusion coefficient (*D**) distributions (normalized to maximum values).

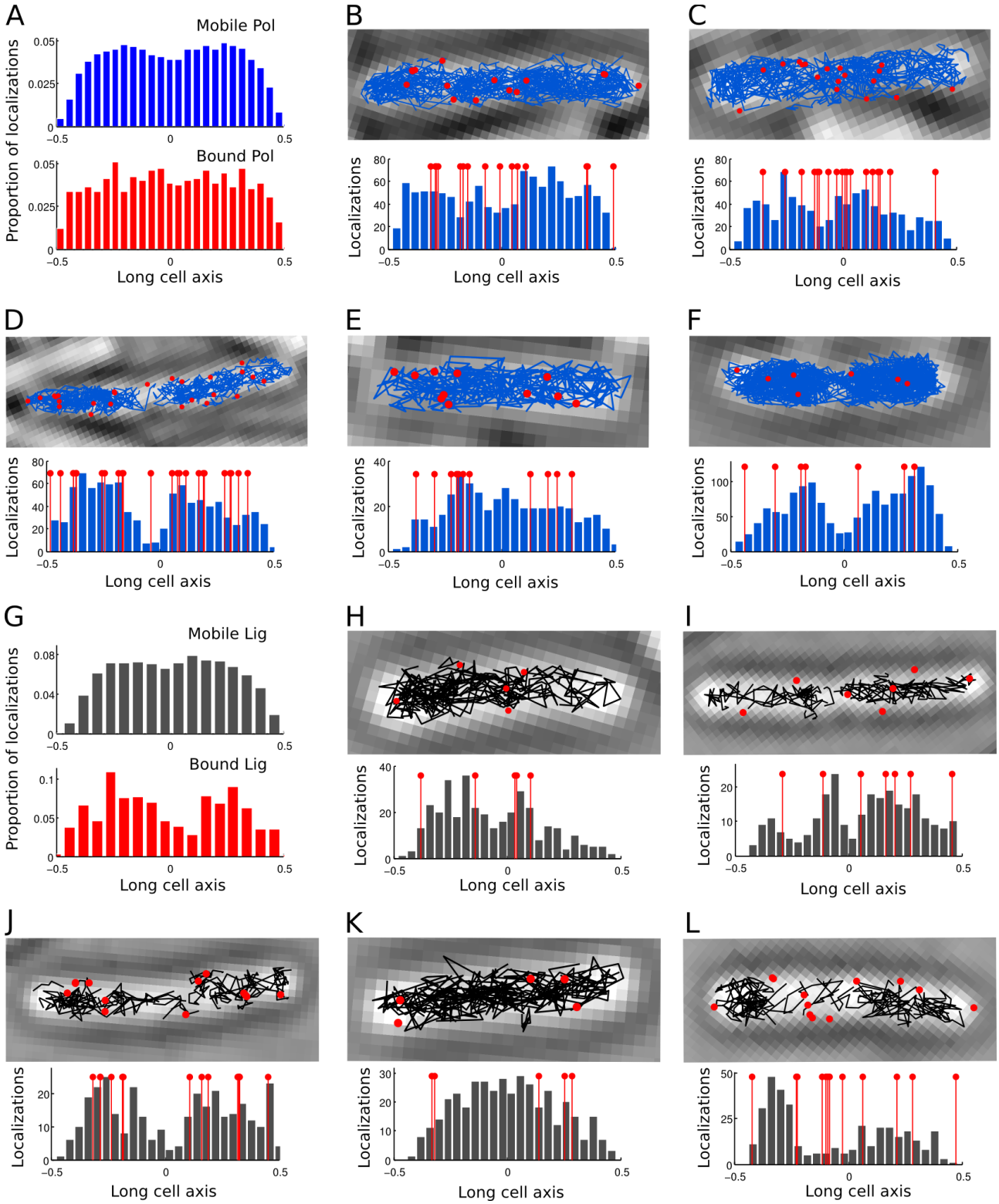

Fig. S5. The spatial distribution of Pol and Lig repair sites with 100 mM MMS is uniform across the nucleoid. (*A*) Projection of the distribution of mobile Pol localizations (top) and bound Pol localizations (bottom) onto the normalized long cell axis (combined data from 95 cells). (*B-F*) Top: Example cells with diffusing Pol (blue tracks) and mean positions of bound Pol (red dots). Bottom: Projection of mobile Pol localizations onto the normalized long cell axis for the cell shown above. Mean localizations of bound Pol are shown in red. (*G-L*) Spatial distribution of Lig DNA repair sites (data displayed as for Pol).

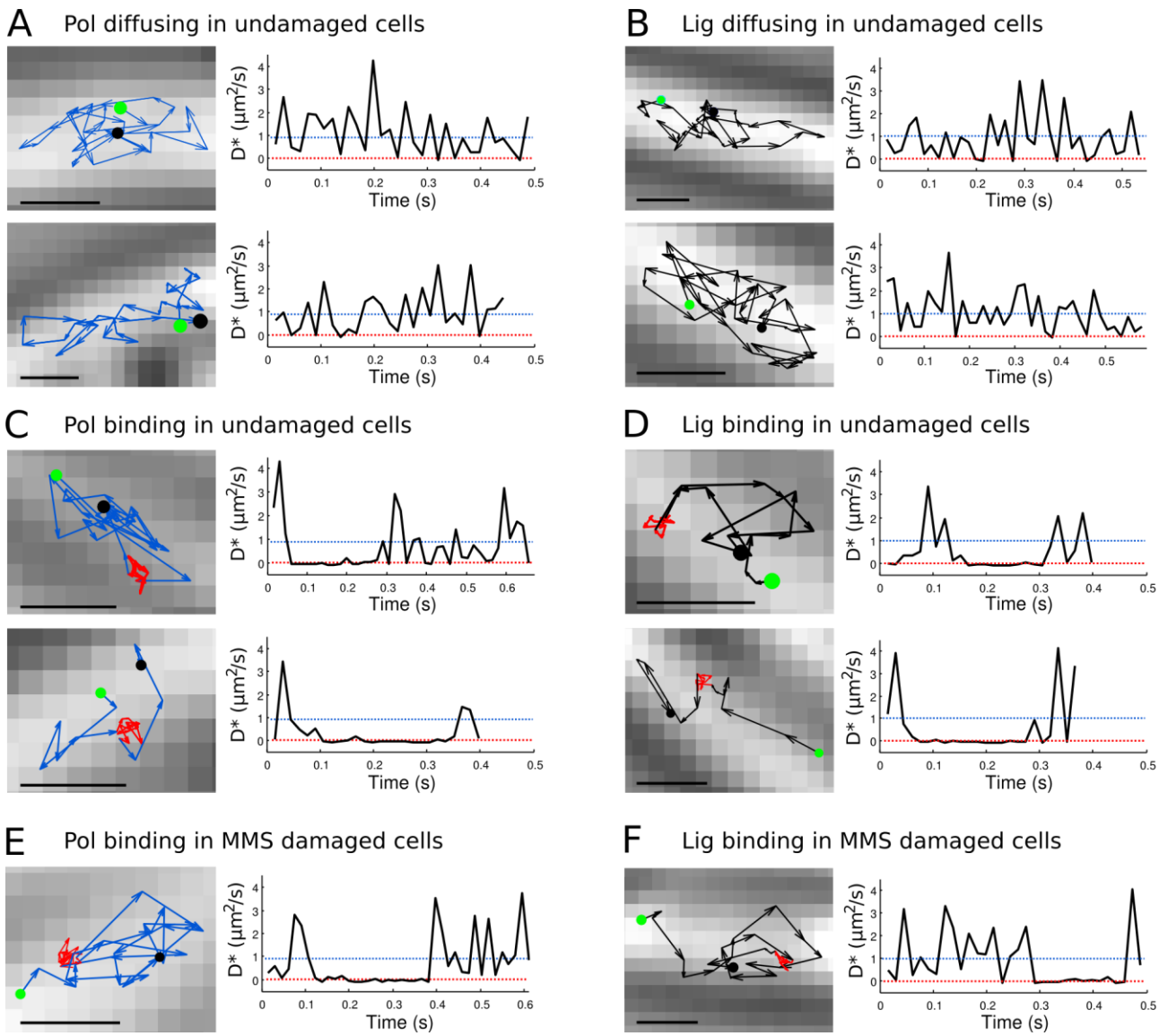

Fig. S6. Further examples of Pol and Lig binding events in undamaged cells and under 100 mM MMS treatment. (*A-B*) Example tracks (starting at green dot, finishing at black dot) and time traces of the diffusion steps showing Pol and Lig movement in undamaged cells. Dotted blue and red lines indicate the average *D** for mobile and bound molecules. (*C-D*) Example Pol and Lig tracks and time traces showing full binding events (highlighted as red arrows) flanked by diffusion in undamaged cells. (*E-F*) Example Pol and Lig tracks and time traces showing full binding events (red arrows), flanked by diffusion in MMS-damaged cells. Scale bars: 0.5 μm.

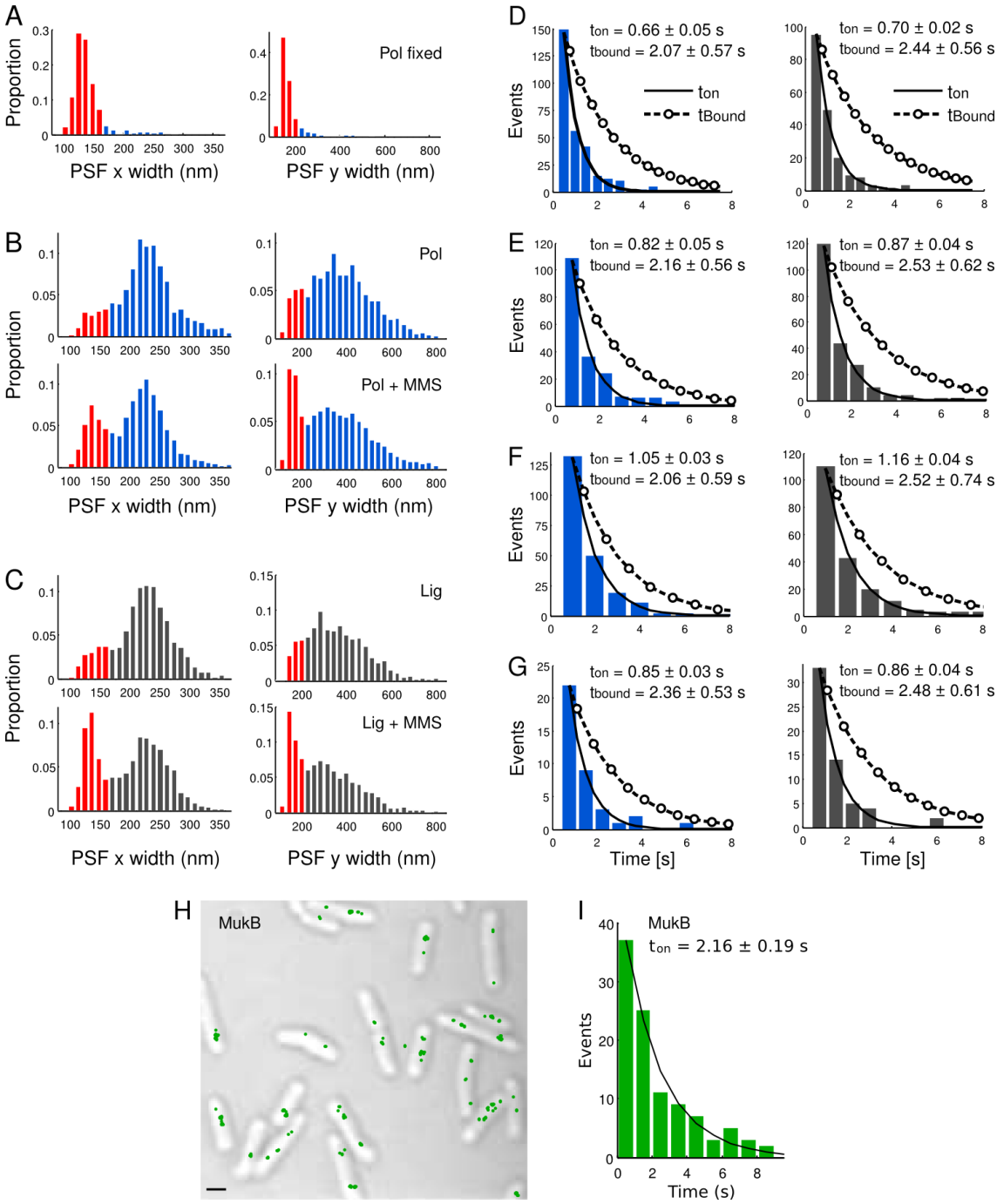

Fig. S7. Measuring binding times. (*A-C*) Fitted elliptical Gaussian PSF width at 750-ms exposures (fit parameters: x width, y width, and rotation angle; x width was assigned to the shorter elliptical axis). (*A*) Pol in fixed cells showed exclusively narrow PSFs. (*B*) Pol in undamaged cells showed blurred PSFs of diffusing molecules. 100 mM MMS treatment increased the population of narrow PSFs. (*C*) Lig in undamaged cells and with 100 mM MMS treatment. (*D-G*) On-time distributions for Pol (left column) and Lig (right column) with 100 mM MMS measured at different exposure times and excitation intensities. Solid lines are exponential fits to the on-time distributions for bound molecules (t_{on} ± SD). Dashed lines with circles are the binding-time distributions (t_{bound} ± SD), recovered by correcting t_{on} for photobleaching t_{bleach} of PAmCherry (Table S3). Curves were normalized by maximum value. (*D*) 500 ms exposure time, 80 W·cm^{-2}excitation intensity. (*E*) 750 ms, 60 W·cm^{-2}. (*F*) 1000 ms, 40 W·cm^{-2}. (*G*) 750 ms, 60 W·cm^{-2}; undamaged cells. (*H*) Independent measure of the photobleaching rate in live cells using MukE-PAmCherry. Clusters of bound MukE (green dots; as reported before: Ref. 17) are shown on a transmitted light microscopy image. (*I*) t_{on} distribution for bound MukE-PAmCherry (1000 ms exposure, 40 W·cm^{-2} excitation; same conditions as for Pol and Lig in panel *F*). Because MukE unbinding is slow (~50 s; Ref. 17) compared to photobleaching, t_{on} matches the photobleaching time t_{bleach} = 2.15 ± 0.15 s measured for Pol-PAmCherry in fixed cells (Table S3). This confirms that the PAmCherry photobleaching rates are similar in live and fixed cells.

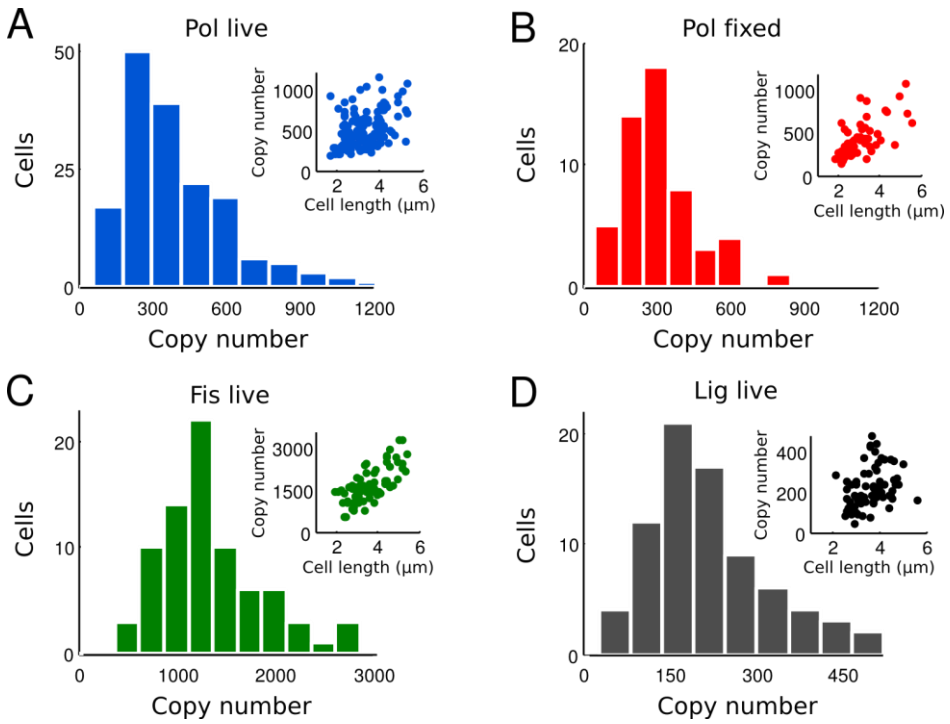

Fig. S8. Protein copy numbers per cell. (*A*) Pol-PAmCherry in live *E.coli* (median value 479). (*B*) Pol-PAmCherry in fixed *E.coli* (median value 421). (*C*) Fis-PAmCherry in live *E.coli* (median value 1560). (*D*) Lig-PAmCherry in live *E.coli* (median value 226). Insets show copy numbers as a function of the cell length.

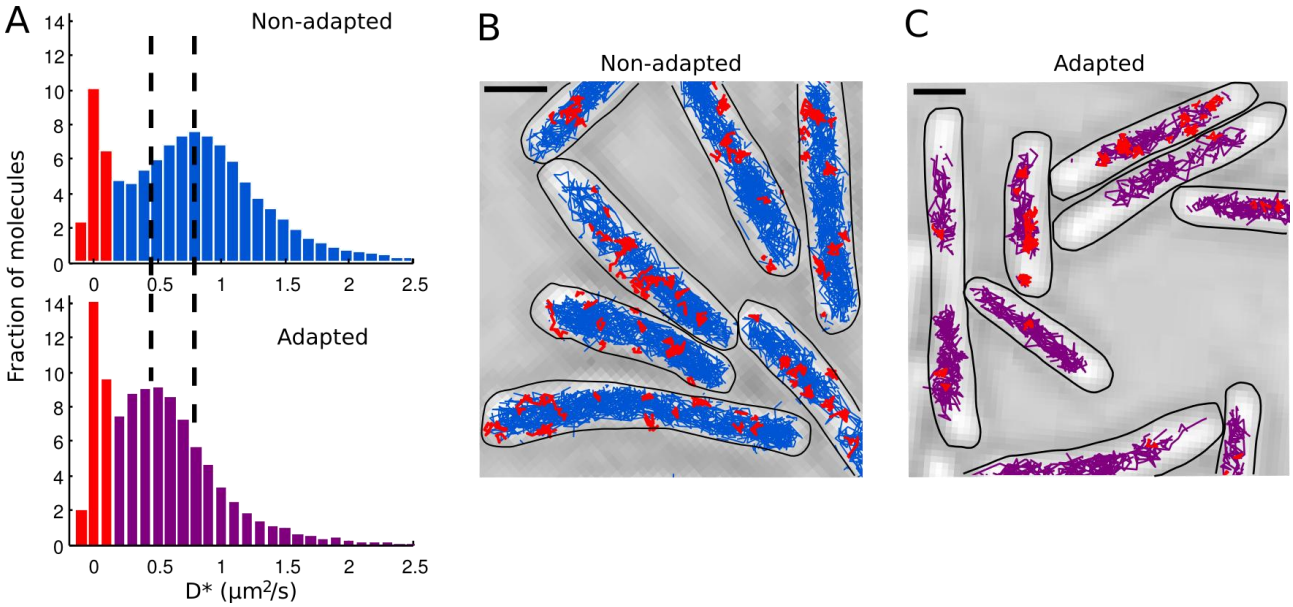

Fig. S9. Influence of the adaptive response to MMS damage on Pol diffusion and binding. The adaptive response was induced with 3 mM MMS for 1 h and adapted cells were measured subsequently under constant 100 mM MMS treatment identical to non-adapted cells. (*A*) Apparent diffusion coefficient (*D**) distributions for Pol in non-adapted cells (top, blue) and in adapted cells (bottom, magenta). Adaptation leads to increased Pol binding under saturating MMS treatment (18.6 ± 0.2 % in adapted cells vs. 13.0 ± 0.2 % in non-adapted cells). The shift of the unbound Pol population to lower *D** values in adapted cells (shown by vertical dashed lines) indicates compaction and increased viscosity of the nucleoid upon adaptation. N > 10,000 tracks; populations of bound molecules are shown in red. (*B*) Pol tracks in non-adapted cells and (*C*) in adapted cells with 100 mM MMS. Diffusing tracks in blue/magenta, bound tracks in red. The spatial distribution of the tracks reflects the size and position of the nucleoid, which appears more compacted in adapted cells. Scale bars: 1 μm.

	Sequence
Lambda polA-F	TGCCGTTGCTGGTGGAAGTGGGGAGTGGCGAAAACTGGGATCAGGC GCACTCGGCTGGCTCCGCTGC
Lambda polA-R	GTGACAGCTTATGTTGCTTACTTACGAAAAAAGGCATGTTCAGGCGAA TCCTTATGAATATCCTCCTTAG
Lambda ligA-F	TGGGCATTGAAGTCATCGACGAAGCGGAAATGCTGCGTTTGCTGGGT AGCTCGGCTGGCTCCGCTGCTGG
Lambda ligA-R	CAAACGGCATTATCGTATTGGCTATTTCAATCAGCTGCTCTTTTTCCAT CCTTATGAATATCCTCCTTAG
Lambda fis-F	GCATCAACCGTGGTACGCTGCGTAAAAAATTGAAAAAATACGGCATG AACTCGGCTGGCTCCGCTGCTGG
Lambda fis-R	TCCCCATGCCGAGTAGCGCCTTTTTAATCAAGCATTTAGCTAACCTGAA TCTTATGAATATCCTCCTTAGTTCC
polA seqF	GAAGCGCAGAAGTACATGGA
polA seqR	TGCTTGTGCCGGATGTGGC
ligA seqF	TTCGGCACGCTGGAAGCG
ligA seqR	AGACCGAACAGTTACAGGC
fis seqF	ATCTGGACACTGGGGAGTTG
fis seqR	ATCACTTCAAACAGCCAGTGC

Table S1. Primers used in the construction and characterization of strains carrying PAmCherry fusions.

	AB1157 wild type	*polA-PAmCherry*	*ligA-PAmCherry*	*fis-PAmCherry*
LB (min)	28.7	29.7	28.8	28.4
M9 glycerol (min)	86.6	87.7	88.8	84.5

Table S2. Growth rates at 37ºC.

	500 ms, 80 W·cm^{-2} + MMS	750 ms, 60 W·cm^{-2} + MMS	1000 ms, 40 W·cm^{-2} + MMS	750 ms, 60 W·cm^{-2} no MMS
t_{bleach} [s]	0.97 ± 0.04	1.33 ± 0.06	2.15 ± 0.15	1.33 ± 0.06
Pol t_{on} [s]	0.66 ± 0.05	0.82 ± 0.05	1.05 ± 0.03	0.85 ± 0.03
Pol t_{bound} [s]	2.07 ± 0.57	2.16 ± 0.56	2.06 ± 0.59	2.36 ± 0.53
Lig t_{on} [s]	0.70 ± 0.02	0.87 ± 0.04	1.16 ± 0.04	0.86 ± 0.04
Lig t_{bound} [s]	2.44 ± 0.56	2.53 ± 0.62	2.52 ± 0.74	2.48 ± 0.61

Table S3. Exponential time constants for PAmCherry photobleaching t_{bleach}, measured on-times t_{on}, and corrected binding times t_{bound} for Pol and Lig with 100 mM MMS treatment (columns 1-3) and without MMS treatment (column 4) (±SD).